Strojniški vestnik - Journal of Mechanical Engineering 70(2024)9-10, 440-451
DOI:10.5545/sv-jme.2023.908
Original Scientific Paper
Received for review: 2023-12-27
Received revised form: 2024-04-04
Accepted for publication: 2024-05-20


# Kurtosis Control of Amplitude-Modulated non-Gaussian Signals for Fatigue Test

Fei Xu[1,*] – Huixian Yang[1] – Kjell Ahlin[2] – Zhifeng Chen[1]
[1] Yancheng Institute of Technology, China
[2] Xielalin Consulting, Sweden

*The amplitude modulation method was used to generate non-Gaussian signals that acted as excitation for fatigue tests. The fatigue life of structures under non-Gaussian excitation has been proven to be closely related to the features of the amplitude modulation signal (AMS) and kurtosis of the structural response. In this study, the modelling of the AMS by Beta and Weibull distributions and the resulting kurtosis range problem is first reviewed. To solve this problem, a new method for creating an AMS based on a linear combination of Beta and Weibull distributions is proposed. To ensure that the high kurtosis of the amplitude-modulated non-Gaussian signal is correctly transferred to the structural response, the method is further developed to fulfil the specifications for the fatigue damage spectrum (FDS) by controlling the spectral content of the AMS. Herein, a Gaussian AMS with a low-pass cutoff frequency is first generated and then converted to a Weibull or Beta AMS based on the cumulative distribution function (CDF) transformation. The proposed method is verified using simulated and field-measured data. The results show that the full range of specified kurtosis is achieved with the new AMS modelling method. The high kurtosis of the non-Gaussian input signal can be transferred to the linear system response if the mean value of AMS during the period of the system impulse response is the same as AMS.*

**Keywords: non-Gaussian, amplitude modulation method, fatigue damage spectrum, kurtosis**

**Highlights**
- *A new AMS modelling method to solve the kurtosis range problem was introduced.*
- *A criterion based on the period of system impulse response defines slowly varying AMS.*
- *CDF transformation controls the spectral content of AMS.*
- *The low cutoff frequency of AMS ensures high kurtosis transmission.*

## 0 INTRODUCTION

The random vibrations are widely used to test the durability of products. A Gaussian excitation signal characterized by power spectral density (PSD) is produced using modern shaker controllers to evaluate the reliability and fatigue life of products [1], while non-Gaussian random vibration is commonly encountered in practice, e.g., wind-induced vibration [2], road roughness induced vehicle vibration [3], and ocean wave-induced vibration [4]. Various standards for vibration tests indicate that non-Gaussian random vibrations with a kurtosis value greater than 3 lead to a faster fatigue failure in products [5] to [7].

To better evaluate the fatigue damage potential of non-Gaussian random vibrations, several methods have been proposed to generate non-Gaussian signals with given PSD and kurtosis [8] and [9], which can be broadly divided into two families: stationary non-Gaussian with peaks and non-stationary non-Gaussian with bursts [10]. For stationary non-Gaussian signal generation, commonly used methods include the nonlinear transform method [11] and [12], analytical phase manipulation method [13] and filtered Poisson process method [14]. A comprehensive review was presented in [15]. Using the aforementioned methods, an acceleration test can be conducted by increasing the kurtosis while maintaining the same PSD level. However, it has been proved that the high kurtosis of the excitation signal does not necessarily transfer to the system response [16]. According to Rizzi et al. [17], a stationary non-Gaussian excitation results in a Gaussian response in a linear dynamic system. This observation was further investigated by Kihm et al. [18], who demonstrated that for a linear system operating close to the natural frequency, the non-Gaussian excitation results in a Gaussian response when the rate of peaks in the excitation is smaller than the period of the systems impulse response.

In contrast, it has been shown that the high kurtosis of non-stationary non-Gaussian excitation is more easily transferred to the system response, resulting in greater fatigue damage compared to the damage by stationary non-Gaussian excitation [10].

The amplitude modulation method for generating non-stationary, non-Gaussian signals with bursts was first developed by Smallwood [19]. A stationary Gaussian signal was generated and then multiplied with a slowly varying amplitude modulation signal that was independent of the Gaussian signal. The

*Corr. Author's Address: Yancheng Institute of Technology, China, ycit_xufei@163.com

convolution of a Hanning window function and an impulse train with a Beta-distributed amplitude were used to create an amplitude modulation signal (AMS). The kurtosis of a non-stationary signal generated using this method was governed by four parameters of the AMS. However, it is not practical to consider four parameters together to reach a specified kurtosis; the parameters b and L are often set to zero. This assumption does not always correspond to the field-measured non-Gaussian data. To simplify the AMS modelling, Xu et al. [20] used a two-parameter Weibull distribution to model the AMS based on the probability density function (PDF) of the running root mean square (RMS) of the field-measured data. Xu indicated that when modelling the AMS by the Weibull distribution, inappropriate determination of the number of bursts may lead to distortion of the original PSD [21]. The Weibull and Beta distribution method was later further developed to include a theoretical relationship between the kurtosis of the AMS and the parameters of the Weibull/Beta distribution [22]. Using stationary and non-stationary excitation, Braccesi et al. [23] investigated the transfer of kurtosis to the system response. Furthermore, the fatigue damage spectrum (FDS) was utilized to evaluate the damage potential of field-measured non-Gaussian signals [24]. Using FDS as the criterion, Cornelis et al. [25] simulated non-Gaussian random vibrations on a shaker and analysed the transfer of the non-Gaussian characteristics of the excitation signal through a linear system.

The problem with the current simplified Weibull and Beta distribution method is the limited kurtosis range and how to ensure the high kurtosis is correctly transferred to the structural response during the construction of AMS. In this paper, the kurtosis range problem when modelling the AMS by Weibull and Beta distributions is first revealed. A new linear combination method is then presented to address this problem. A criterion based on the AMS's running mean value during the system impulse response period is then proposed to answer the question of under which condition a non-Gaussian signal can be regarded as slowly varying. The new method is finally developed to ensure the high kurtosis of the generated non-Gaussian signal is transferred to the structural response by controlling the spectral content of the AMS.

The remainder of this study is organized as follows. In Section 1, the theoretical background of random signal properties, two commonly used amplitude modulation methods and the FDS calculation process are presented. The kurtosis range problem is revealed for the Weibull and Beta distribution methods. In Section 2, a novel AMS modelling method is presented to address the kurtosis range problem. The method is further developed to control kurtosis transmission based on spectral control and cumulative distribution function (CDF) transformation of the AMS. In Section 3, simulated and field-measured data are used to validate the proposed approach. The field data was measured on a dummy box installed on a mast, using a triaxial accelerometer. Finally, the conclusions are presented in Section 4.

## 1 THEORETICAL BACKGROUND

### 1.1 Gaussian and non-Gaussian Random Signals

The $n^{th}$-order central moment of random signal $x(t)$ can be calculated as follows:

$$m_n = \frac{1}{N}\sum_{i=1}^{N}\left(x_i - \mu\right)^n, \tag{1}$$

where $\mu$ is the mean value, and $N$ is the number of data samples.

The skewness and kurtosis are used to characterize the non-Gaussian characteristics of a random signal.

$$S = \frac{m_3}{\sigma^3}, \tag{2}$$

$$K = \frac{m_4}{\sigma^4}, \tag{3}$$

$$\sigma^2 = m_2 = \frac{1}{N}\sum_{i=1}^{N}\left(x_i - \mu\right)^2, \tag{4}$$

where $\sigma$ is the standard deviation, $S$ is the skewness, and $K$ is the kurtosis.

For a Gaussian signal, the skewness is 0, and the kurtosis is 3. The PDF of signals with different kurtosis values is shown in Fig. 1 in semi-log coordinates.

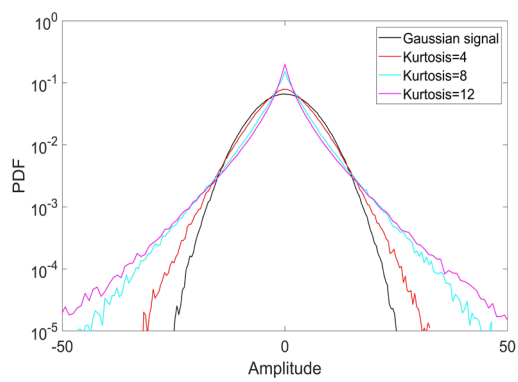


**Fig. 1.** *PDFs of signals with different kurtosis values*

From Fig. 1, we can see that a kurtosis value greater than 3 indicates a sharper peak and wider tails relative to a Gaussian distribution. A wider tail indicates a higher probability of peak values, which leads to larger fatigue damage and faster failure.

### 1.2 Overview of the Amplitude Modulation Method

The essential idea behind the amplitude modulation method is to model non-Gaussian signal $y(t)$ using Gaussian signal $g(t)$ multiplied by a slowly varying AMS $w(t)$:

$$y(t) = g(t) \cdot w(t). \tag{5}$$

To make the PSD of the non-Gaussian signal approximately the same as that of the Gaussian signal, the mean square of the AMS is scaled to one. Assuming that the mean of the Gaussian and non-Gaussian signals is zero and that the Gaussian signal is independent of the AMS, the kurtosis of the non-Gaussian signal is:

$$K_y = \frac{E\left(y^4\right)}{E\left(y^2\right)\cdot E\left(y^2\right)} = \frac{E\left(\mathrm{g}^4 \cdot w^4\right)}{E\left(g^2 \cdot w^2\right)\cdot E\left(g^2 \cdot w^2\right)} = \frac{E\left(\mathrm{g}^4\right)\cdot E\left(w^4\right)}{E\left(g^2\right)\cdot E\left(g^2\right)\cdot E\left(w^2\right)\cdot E\left(w^2\right)} = 3 \cdot K_w, \tag{6}$$

where $K_w$ is the kurtosis of $w(t)$ obtained with the mean value, which can be calculated as:

$$K_w = \frac{\frac{1}{N}\sum_{i=1}^{N} w_i^4}{\frac{1}{N}\sum_{i=1}^{N} w_i^2 \cdot \frac{1}{N}\sum_{i=1}^{N} w_i^2} = N \cdot \frac{\sum_{i=1}^{N} w_i^4}{\sum_{i=1}^{N} w_i^2 \cdot \sum_{i=1}^{N} w_i^2}. \tag{7}$$

Clearly, the kurtosis of the generated non-Gaussian signal depends on that of the AMS. The Weibull distribution [21] and Beta distribution [19] are commonly used to simulate AMS, and it has been concluded that the generated non-Gaussian signal retains the same properties as the field data.

#### 1.2.1 Weibull Distribution

The PDF of AMS $w(t)$ following a Weibull distribution is defined as:

$$f\left(w,\lambda,k\right) = \begin{cases} \frac{k}{\lambda}\left(\frac{w}{\lambda}\right)^{k-1} \cdot e^{-\left(\frac{w}{\lambda}\right)^k} & w \geq 0 \\ 0 & w < 0 \end{cases}, \tag{8}$$

where $k$ is the shape parameter, and $\lambda$ is the scale parameter.

The average of powers of $w(t)$ is:

$$E\left(w^n\right) = \lambda^n \cdot \Gamma\left(1+\frac{n}{k}\right), \tag{9}$$

where $\Gamma$ is the gamma function.

According to Eq. (6), the kurtosis of the non-Gaussian signal is:

$$K_y = \frac{E\left(w^4\right)}{E\left(w^2\right)\cdot E\left(w^4\right)} \cdot 3 = \frac{\Gamma\left(1+\frac{4}{k}\right)}{\left(\Gamma\left(1+\frac{2}{k}\right)\right)^2} \cdot 3. \tag{10}$$

Using Eq. (10), the shape parameter $k$ can be obtained once the kurtosis of the non-Gaussian signal (target kurtosis) has been given. Fig. 2 shows the relationship between target kurtosis and shape parameter when the kurtosis is increased from 3 to 12.

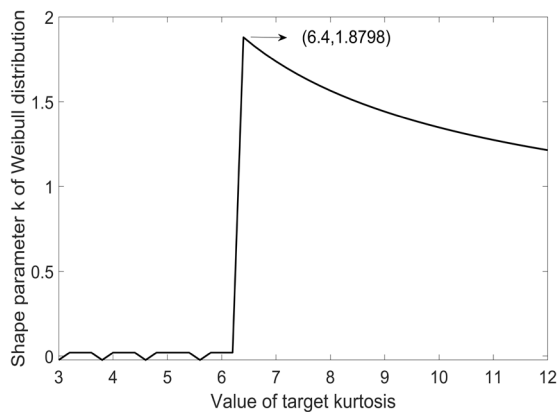


**Fig. 2.** *Relationship between target kurtosis and shape parameter k*

As shown in Fig. 2, when target kurtosis is below 6.4, $k$ is close to 0, indicating that the Weibull distribution method applies only when target kurtosis is above 6.4, and the corresponding range of the shape parameter $k$ is [1.28, 1.88].

#### 1.2.2 Beta Distribution

The PDF of AMS $b(t)$ following a Beta distribution is defined as:

$$f\left(b,\alpha,\beta\right) = \frac{\Gamma\left(\alpha+\beta\right)}{\Gamma\left(\alpha\right)\cdot\Gamma\left(\beta\right)} \cdot b^{\alpha-1} \cdot \left(1-b\right)^{\beta-1}. \tag{11}$$

The Beta distribution is determined by the two positive values, $\alpha$ and $\beta$.

The average of powers of $b(t)$ is:

$$E\left(b^{n}\right)=\prod_{i=0}^{n-1}\frac{\alpha+i}{\alpha+\beta+i}. \tag{12}$$

The skewness of the AMS with a Beta distribution is:

$$S=\frac{2(\beta-\alpha)\sqrt{\alpha+\beta+1}}{(\alpha+\beta+2)\sqrt{\alpha\beta}}. \tag{13}$$

Typically, the skewness of the signal is 0; thus, $\alpha=\beta$. The kurtosis of the non-Gaussian signal is:

$$K_{y}=\frac{4\beta^{3}+22\beta^{2}+34\beta+12}{4\beta^{3}+14\beta^{2}+16\beta+6}\cdot 3. \tag{14}$$

Fig. 3 shows the relationship between target kurtosis and the parameter $\beta$. As can be observed, when target kurtosis is above 6.05, the value of $\beta$ is negative, which is forbidden. Thus, the reasonable range of β is $[0, 10.7]$.

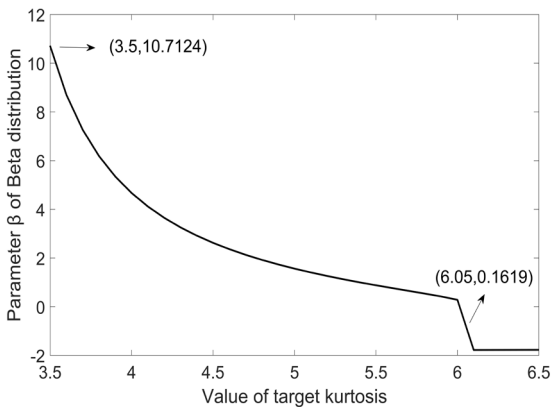


**Fig. 3.** *Relationship between target kurtosis and parameter $\beta$*

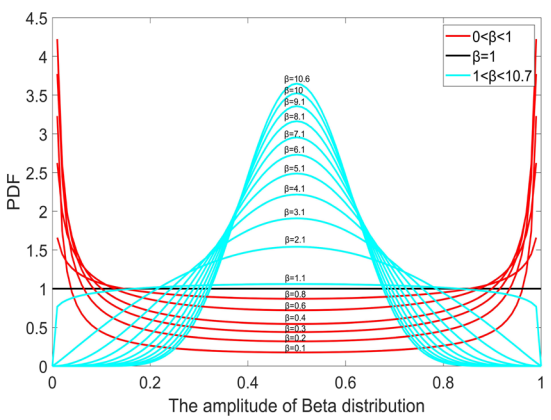


**Fig. 4.** *PDF of Beta distribution with parameter $\beta$ in the range [0, 10.7]*

Fig. 4 shows the PDF when β is in the range $[0, 10.7]$. As can be observed, the shape of the PDF changes for different values of β. When $0<\beta<1$, the PDF has a bimodal shape, which is not useful here. When $\beta=1$, the PDF is a straight line, and the kurtosis is 5.4. When $\beta>1$, the PDF follows a Beta distribution. Above all, the Beta distribution method is limited to a kurtosis value of up to 5.4, and the β is in the range $[1, 10.7]$. To make the PSD for the non-Gaussian signal basically the same as that for the Gaussian signal, the mean square of the AMS is also scaled to one.

### 1.3 Fatigue Damage Spectrum (FDS)

FDS is commonly used to evaluate the damage potential of field-measured non-Gaussian signals. As shown in Fig. 5, the FDS is calculated based on the responses of a series of single-degree-of-freedom (SDOF) systems to the same base excitation, thereby showing the fatigue damage encountered for a particular SDOF system within a certain time duration [21].

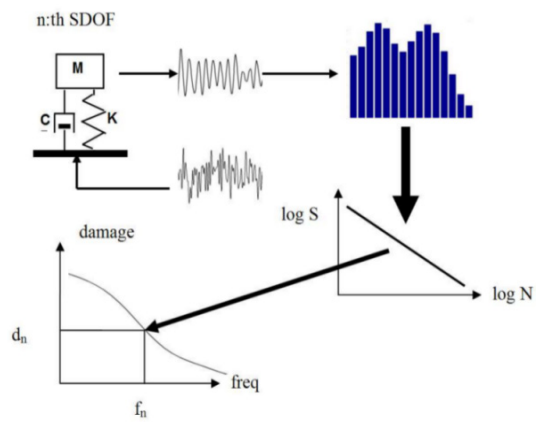


**Fig. 5.** *Calculation process of the FDS*

The stress is assumed to be roughly proportional to pseudo-velocity in this study [26]. For an SDOF system with a natural frequency fn and a damping ratio ζ, the output pseudo-velocity xpv to an input acceleration xa can be calculated:

$$x_{pv}=F_{filter}\left(b_{n},a_{n},x_{a}\right), \tag{15}$$

where $F_{filter}$ indicates filtering of the input signal using a ramp invariant digital filter, $b_n$ and $a_n$ are the coefficients of a digital filter [27].

Using the output $x_{pv}$, the cumulative damage can be calculated in both time and frequency domains. In the time domain, a faster algorithm than the rain flow cycle counting (RFCC) method [28] is used to calculate the total damage index $D_t$. It starts by

converting the output pseudo-velocity into a peak-valley signal, where the data points between the maxima and minima are deleted. Each maximum $x_{pv,pk,i}$ is regarded as the peak value of a cycle with the range $2x_{pv,pk,i}$. The minima are counted in the same manner, and the sum is divided by 2.

$$D_t = \sum_{i=1}^{q} \frac{\left|S_{pk,i}\right|^b}{2c} = \sum_{i=1}^{q} \frac{k^b \left|x_{pv,pk,i}\right|^b}{2c}, \quad (16)$$

where $S_{pk,i}$ ($i = 1, 2, ..., q$) is assumed to be proportional to the maximum and minimum values $x_{pv,pk,i}$ and $q$ is the number of maximum and minimum values considered, and $b$ is the fatigue exponent.

Whereas for exact fatigue life predictions, $c$ and $k$ have to be known explicitly, in practice, their values may be unknown or difficult to estimate. In this case, it is possible to set $c = k = 1$ and nevertheless use the FDS as an indicator to compare the damage potential of different vibration profiles [29].

In the frequency domain, the total damage is calculated as [22]:

$$D_f = \frac{f_n T}{c}\left(2\sigma_S^2\right)^{b/2}\Gamma\left(1+\frac{b}{2}\right) = \frac{f_n T}{c}k^b\left(2\sigma_{pv}^2\right)^{b/2}\Gamma\left(1+\frac{b}{2}\right), \quad (17)$$

where $T$ is the total time of exposure to the stress environment, $\Gamma$ is the Gamma function, $\sigma_S$ is the RMS of the stress time history, and $\sigma_{pv}$ is the RMS of pseudo-velocity.

The frequency domain method has many advantages, such as reduced computation time. However, it only applies when the excitation is a Gaussian signal [22].

## 2 NOVEL AMS MODELLING METHOD

### 2.1 Linear Combination Method to Model the AMS

As mentioned in Section 1.2.1, the Weibull distribution is suitable for generating non-Gaussian signals with a kurtosis greater than 6.4, whereas the Beta distribution is applicable for a kurtosis range of [3, 5.4]. To fill the gap in the kurtosis range of [5.3, 6.5], a new method based on a linear combination of the two aforementioned modulation signals is proposed.

The modulation signal, $b(t)$, is generated by the Beta distribution and the other modulation signal, $w(t)$, is generated by the Weibull distribution. The linear superposition of the two modulation signals is then used to create a new amplitude modulation signal, $s(t)$.

$$s(t) = m \cdot b(t) + n \cdot w(t). \quad (18)$$

Since kurtosis of $s(t)$ is the same as kurtosis of $s(t)/n$, $n$ is set 1 in this paper. According to Eq. (6), the kurtosis of the modulation signal, $s(t)$, is:

$$K_s = \frac{E\left[\left(m\cdot b + w\right)^4\right]}{E\left[\left(m\cdot b + w\right)^2\right]\cdot E\left[\left(m\cdot b + w\right)^2\right]} = \frac{E\left(m^4\cdot b^4\right)+E\left(w^4\right)+E\left(6m^2\cdot b^2\cdot w^2\right)+E\left(4m\cdot b\cdot w^3\right)+E\left(4m^3\cdot b^3\cdot w\right)}{\left[E\left(m^2\cdot b^2\right)+E\left(w^2\right)+E\left(2m\cdot b\cdot w\right)\right]^2}, \quad (19)$$

$$K_s = \frac{E\left(b^4\right)m^4 + 4E\left(b^3\right)E\left(\mathrm{w}\right)m^3 + 6m^2 + 4E\left(b\right)E\left(\mathrm{w}^3\right)m + E\left(w^4\right)}{m^4 + 4E\left(b\right)E\left(\mathrm{w}\right)m^3 + \left[2 + 4\left(E\left(b\right)E\left(\mathrm{w}\right)\right)^2\right]m^2 + 4E\left(b\right)E\left(\mathrm{w}\right)m + 1}. \quad (20)$$

Using the generated $b(t)$ and $w(t)$, parameter m can be calculated according to Eq. (20), as target kurtosis Ks is given. Fig. 6 shows the relationship between m and target kurtosis. Fig. 7 shows the PDF of the modulation signals when target kurtosis is in the range [5.3, 6.5] using the linear combination method.

Thus, it can be concluded that a non-Gaussian signal with a kurtosis value greater than 3 can be simulated based on the three amplitude modulation functions. However, the creation of the AMS must be treated carefully so that a high kurtosis is transferred to the response of the system, causing the expected extra damage in a fatigue test. A new method for controlling the spectral content of the AMS is presented in this paper.

### 2.2 Criterion for Slowly Varying non-Gaussian Signal

For an SDOF system with resonance frequency $f_0$ and damping ratio $\zeta$, the motion of this system is:

$$\ddot{x}(t) + 2\zeta\omega_0\dot{x}(t) + \omega_0^2 x(t) = 2\zeta\omega_0\dot{y}(t) + \omega_0^2 y(t), \quad (21)$$

where $y(t)$ is the base input non-Gaussian signal and $\omega_0$ is the angular natural frequency ($\omega_0 = 2\times\pi\times f_0$).

When the response of the SDOF system is calculated as relative displacement between the SDOF system mass and the base multiplied by the angular natural frequency $\omega_0$, the pseudo-velocity impulse response function, $h(t)$, is [30]:

$$h(t) = \frac{1}{\sqrt{1-\zeta^2}} exp(-\zeta\omega_0 t) sin\omega_d t \quad t \geq 0. \tag{22}$$

The response of the pseudo-velocity filter to an input non-Gaussian signal is:

$$r(t) \approx w_0^2 \cdot \{w(t) \cdot g(t)\} * h(t)$$
$$= w_0^2 \cdot \int_0^T w(t-\tau) \cdot g(t-\tau) \cdot h(\tau) d\tau, \tag{23}$$

where $h(t)$ is the impulse response of a pseudo-velocity filter and '*' denotes convolution.

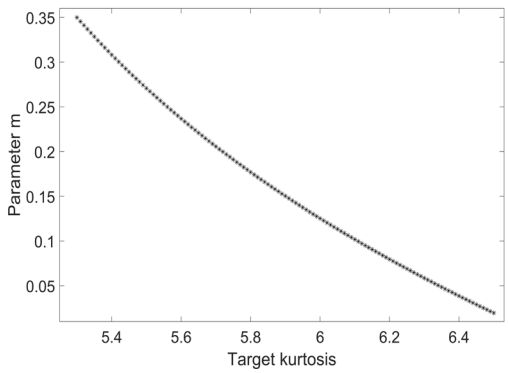


**Fig. 6.** *Relationship between m and target kurtosis*

There is first a transient part in the beginning of the signal; however, after a short period, we only have to look backwards by duration $T$, which is the period of $h(t)$.

If the input non-Gaussian signal varies slowly, the AMS, $w(t)$, can be considered a constant during $T$. Then, we can take $w(t)$ outside the integral in Eq. (23), which indicates that the mean of $w(t)$ during the period of $h(t)$ is the same as $w(t)$; thus, the response is the same as the response of the Gaussian signal, multiplied by $w(t)$:

$$r(t) = w_0^2 \cdot w(t) \cdot \{g(t) * h(t)\}. \tag{24}$$

Because $g(t)*h(t)$ results in a Gaussian signal, from Eq. (24), it can be deduced that the response is also a slowly varying non-Gaussian signal. Therefore, it can be concluded that if the mean value of $w(t)$ during the period of $h(t)$ is the same as $w(t)$, a non-Gaussian signal can be regarded as slowly varying.

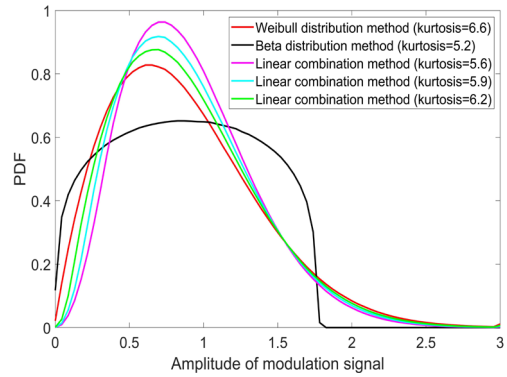


**Fig. 7.** *PDF of modulation signal when target kurtosis is in the range [5.3, 6.5]*

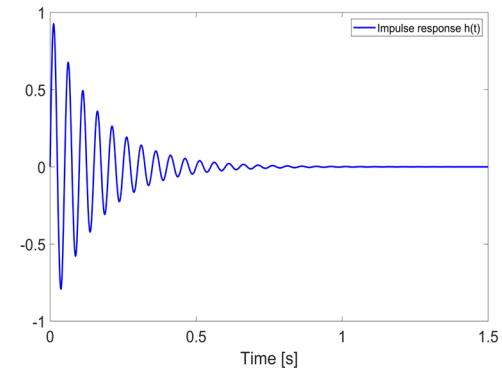


**Fig. 8.** *Pseudo-velocity impulse response function $h(t)$*

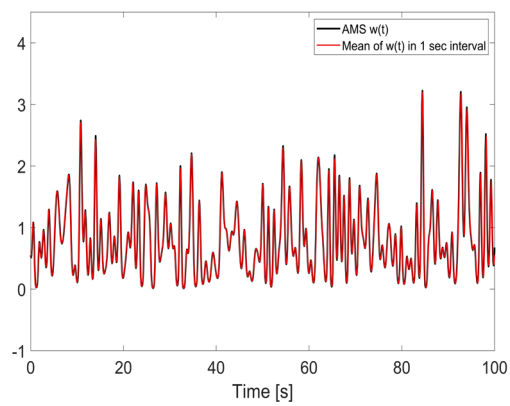


**Fig. 9.** *Comparison between w(t) and mean of $w(t)$*

Assuming an SDOF system with a resonance frequency of 20 Hz and resonance gain factor $Q = 1/(2\zeta) = 10$, the impulse response, $h(t)$, for the pseudo-velocity filter, is shown in Fig. 8. From Fig. 8, we observe that the period of $h(t)$ is approximately 1 s. According to Eqs. (22) to (24), it can be seen that the kurtosis is not relevant in the criterion for slowly varying non-Gaussian signals. The key is to see if the mean value of $w(t)$ during the period of $h(t)$ is the same as $w(t)$. Assuming that the target kurtosis of a non-

Gaussian signal is 9, then the AMS can be modelled using a Weibull distribution. The mean of $w(t)$ in a frame length of 1 s is taken and compared with $w(t)$, and the results are shown in Fig. 9. From Fig. 9, it can be observed that the mean of $w(t)$ is essentially the same as $w(t)$, which indicates that the non-Gaussian signal can be regarded as slowly varying.

### 2.3 Control of the AMS

To ensure that the high kurtosis of the amplitude-modulated signal is correctly transferred to the structural response, the AMS must be slowly varying, which means the frequency content of the AMS must be controlled. However, if the Weibull/Beta approach is used directly to create the AMS and perform low-pass filtering, the PDF of the filtered AMS will change. A better method based on the CDF transformation is proposed in this study to solve this problem. A Gaussian AMS with a cutoff frequency (denoted as $W_{cut}$) is first generated from a flat PSD whose frequency content is easy to control and then converted to a Weibull or Beta signal with given parameters while maintaining the low-pass frequency content. The cutoff frequency can be determined based on the frequency content of the running RMS of the field-measured non-Gaussian data. An example is presented in this paper.

The CDF of a standard Gaussian signal is:

$$F_x = \frac{1}{2}\left[1 + erf\left(\frac{x}{\sqrt{2}}\right)\right], \tag{25}$$

where *erf*() is the error function.

The error function is defined as follows:

$$\mathrm{erf}\left(x\right) = \frac{2}{\sqrt{\pi}}\int_0^x e^{-t^2}\,dt. \tag{26}$$

The Gaussian distribution is then transformed into a Weibull or Beta distribution, depending on the target kurtosis.

The CDF of the Weibull distribution is:

$$CDF_{Weibull} = \begin{cases} 1 - e^{-(x/\lambda)^k} & x \geq 0 \\ 0 & x < 0 \end{cases}. \tag{27}$$

Set $\lambda = 1$; then, the inverse cumulative distribution is:

$$G^{-1}\left(y\right) = \left(-\log\left(1-y\right)\right)^{1/k}. \tag{28}$$

Using Eqs. (25) and (28) and substituting $y$ with $F_x$, the Weibull distribution AMS can be expressed as follows:

$$x_{Weibull} = \left(-\log\left(\frac{1}{2}\left(1 - \mathrm{erf}\left(\frac{x}{\sqrt{2}}\right)\right)\right)\right)^{1/k}. \tag{29}$$

The CDF of the Beta distribution cannot be expressed using elementary functions. Therefore, the inverse CDF cannot be expressed in a simple form.

For the Beta distribution, the AMS can be calculated by computing the inverse incomplete beta function and substituting the variable with $F_x$ in Eq. (25):

$$\mathrm{I}_x(\alpha,\beta) = \frac{1}{Beta(\alpha,\beta)}\int_0^x \mathrm{t}^{(\alpha-1)}(1-t)^{\beta-1}\,dt. \tag{30}$$

For the linear combination of the Weibull and Beta distributions, CDF transformations are performed based on the methods presented above to achieve the final AMS.

In each case, the mean square of AMS is finally scaled to one after CDF transformation.

The required $W_{cut}$ is determined by the fact that the responses after the SDOF filters in the FDS calculation do not become Gaussian because if they do, the FDS will be the same as that for a Gaussian signal with the same PSD. As shown in Fig. 13, the NAVMAT PSD [31] is used as an example, and the target kurtosis value is set to 9. The PDF of the simulated Gaussian and non-Gaussian (using $W_{cut}$ 1 Hz and 100 Hz) is shown in Fig. 10 in semi-log coordinates. The responses of a filter with a resonant frequency of 200 Hz and $Q$ = 10 to the three synthesized signals are calculated. A comparison of the response PDF and Gaussian signal with the same RMS is shown in Fig. 11 in semi-log coordinates. As can be observed, as the $W_{cut}$ increases, the AMS $w(t)$ cannot be considered as a constant during the period of $h(t)$, which will make the response signals tend to be Gaussian.

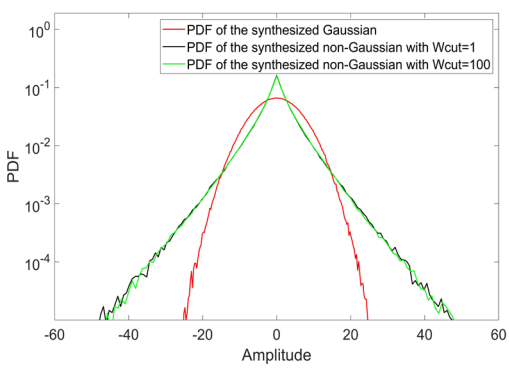


**Fig. 10.** *PDF of synthesized Gaussian and non-Gaussian signals*

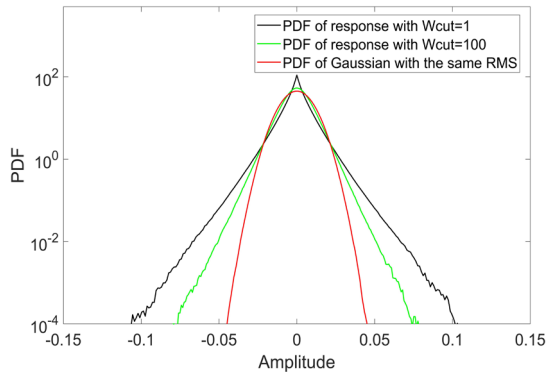


**Fig. 11.** *PDF of response and Gaussian signal with the same RMS*

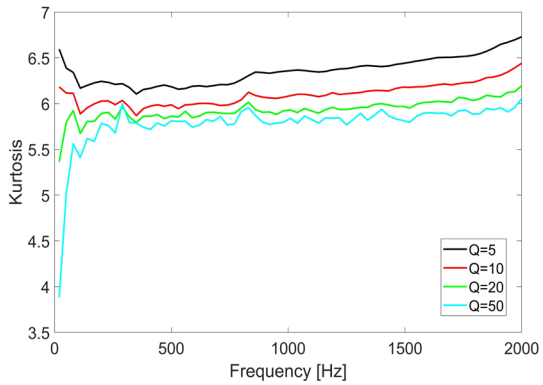


**Fig. 12.** *Effects on the response kurtosis with Q = [5 10 20 50]*

Another factor that affects the non-Gaussianity of the response after the SDOF filters in the FDS calculation is the $Q$ value. Fig. 12 shows the effects of $Q$ on the response kurtosis. We can see from Fig. 12 that the kurtosis decreases as $Q$ increases. The result can be expected, because as $Q$ increases, the damping ratio decreases, and the duration of the impulse response increases. When the duration of the impulse response reaches a certain value, the AMS $w(t)$ cannot be considered as a constant, which will make the response tend to be Gaussian.

## 3 CASE STUDY

### 3.1 Simulated non-Gaussian Signal

The PSD of the NAVMAT profile is shown in Fig. 13. The PSD is defined by the corner points in the frequency and the corresponding PSD values. A frequency record $Z$ is created using the amplitudes as the square roots of the PSD values. Each frequency point is appointed with a random phase in the interval $[0, 2\pi]$. A Gaussian time signal is created using an appropriately scaled IFFT (Inverse Fast Fourier Transform). A stationary Gaussian signal is generated using the MATLAB software. The sampling frequency $Fs$ is 10 kHz, and the number of sampling points $N$ is $2^{20}$. The generated signal is assumed to be an acceleration signal.

$$g(t) = \sqrt{N \cdot Fs/2} \cdot real\left(ifft(Z)\right). \tag{31}$$

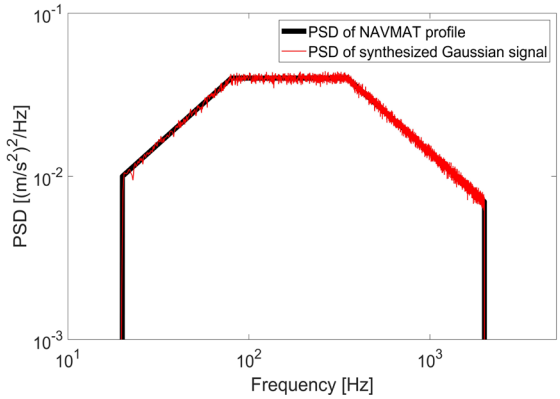


**Fig. 13.** *PSD of NAVMAT profile and synthesized Gaussian signal*

The synthesized Gaussian signal is shown in Fig. 14. The target kurtosis is set to values between 3.5 and 12 in increments of 0.5. The new AMS modelling method is used to generate a non-Gaussian signal. A good agreement between the kurtosis of the target and generated non-Gaussian signals is shown in Fig. 15 ($W_{cut}$ = 1 Hz).

The effects of $W_{cut}$ on the kurtosis of the filter response are shown in Fig. 16. As can be seen, as $W_{cut}$ increases, the kurtosis of the response decreases.

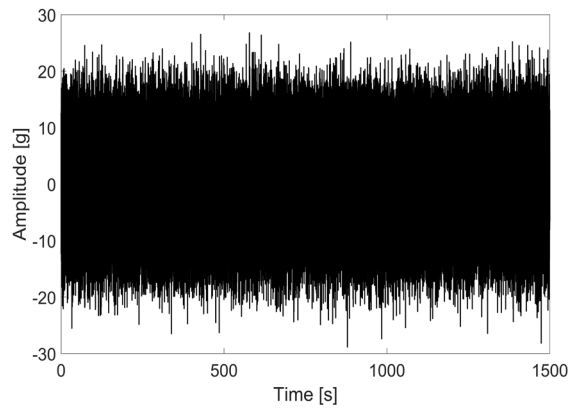


**Fig. 14.** *Synthesized Gaussian signal*

Assuming that target kurtosis is 6, the effects of different $W_{cut}$ on the FDS are shown in Fig. 17. As can be observed in Fig. 17, as $W_{cut}$ increases, the FDS of the simulated non-Gaussian signal decreases, especially over the low-frequency range.

This behaviour can be predicted because as $W_{cut}$ increases, the AMS $w(t)$ varies faster, then the $w(t)$ cannot be regarded as constant during the period of $h(t)$, especially for SDOF systems with lower natural frequencies, which have longer periods of $h(t)$. As a result, the response tends to be Gaussian, and FDS decreases.

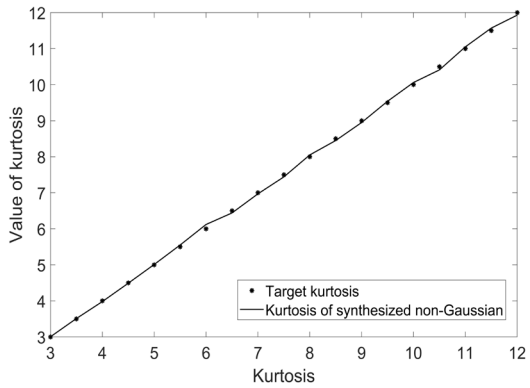


**Fig. 15.** *Target kurtosis and kurtosis of synthesized signal*

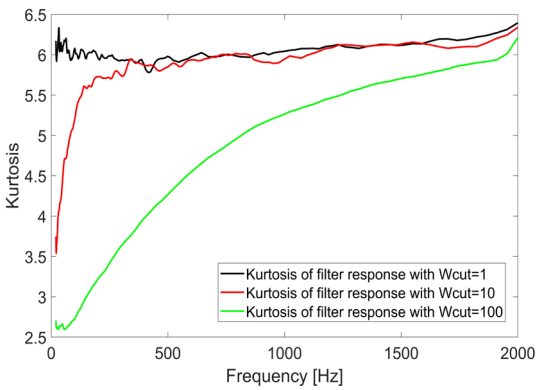


**Fig. 16.** *Effects of $W_{cut}$ [1, 10, 100] on the kurtosis of filter response*

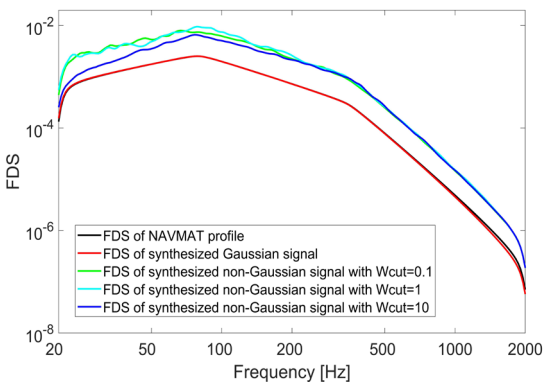


**Fig. 17.** *FDS of NAVMAT profile PSD, and synthesized Gaussian and non-Gaussian signals with $W_{cut}$ = [0.1 1 10]*

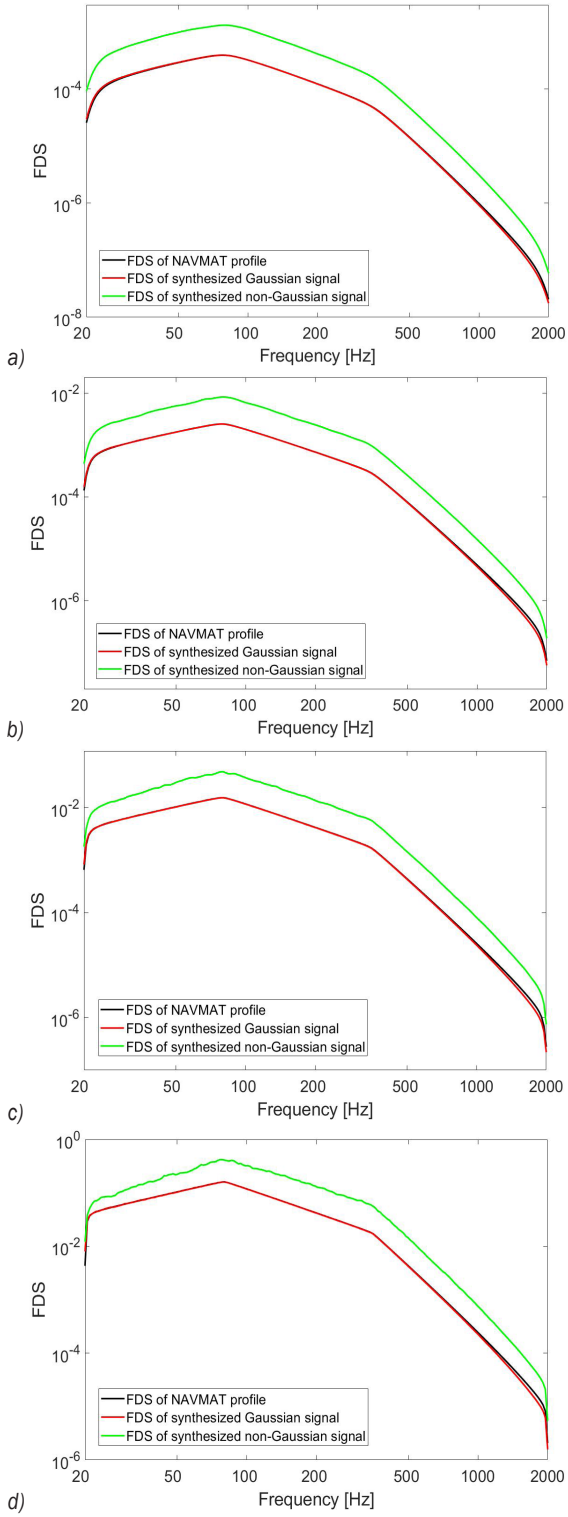


**Fig. 18.** *Effects of $Q$ on FDS; at a) $Q$ = 5, b) $Q$ = 10, c) $Q$ = 20, and d) $Q$ = 50*

Fig. 18 shows the effects of $Q$ on the FDS. From Fig. 18, we can see that, overall, the FDS increases as

$Q$ increases. But, as the $Q$ value increases, the FDS of a non-Gaussian signal tends to be close to the FDS of a Gaussian signal. The reason is that a higher $Q$ value leads to a longer period of $h(t)$, especially for SDOF systems with lower natural frequencies. Then, the $w(t)$ cannot be regarded as constant during the period of $h(t)$. As a result, the response tends to be Gaussian, leading to a smaller kurtosis and lower FDS.

### 3.2 Field-Measured non-Gaussian Signal

In this case study, the field-measured signal induced by wind is used to validate the proposed method. The test item is a dummy box containing electronics installed on a mast, as shown in Fig. 19. The dummy box was equipped with a B&K WB0179 triaxial accelerometer set and a wind speed measuring device. The box was a standard Ericsson micro-radio base equipment manufactured in cast lightweight alloy with integrated heat sinks. The dimensions are about 530 mm × 400 mm × 185 mm, and the weight was about 21 kg. The back side of the dummy box was mounted to the mast at a height of 50 meters. The running RMS is calculated using 10 s frames with 50 % overlapping.

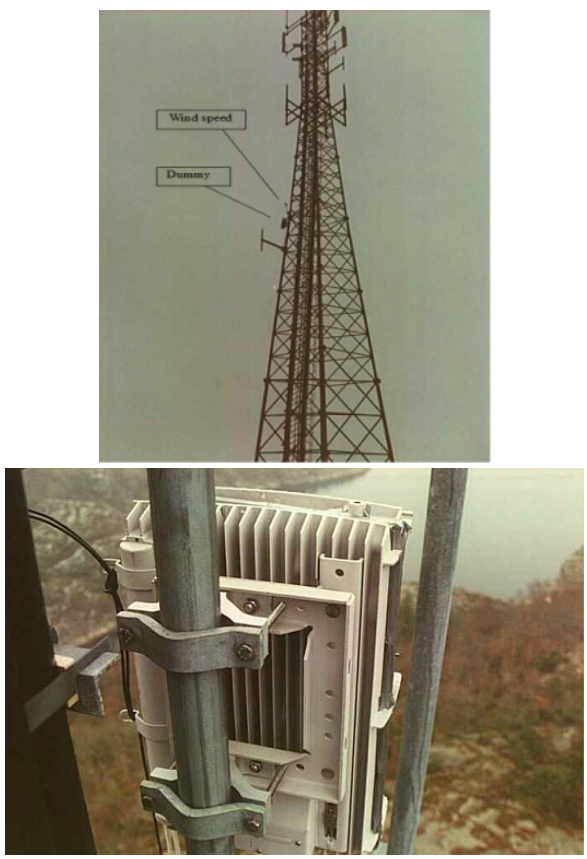


**Fig. 19.** *Test item and setup*

The field data, along with the running RMS, are shown in Fig. 20, which indicates a kurtosis of 5.635. The PSD of the running RMS is shown in Fig. 21. As can be observed from Fig. 21, the upper frequency limit is approximately 0.01 Hz; thus, the $W_{cut}$ is set to 0.01 Hz. The simulated AMS is shown in Fig. 22. A synthesized non-Gaussian signal with a kurtosis of 5.597 is also shown in Fig. 20.

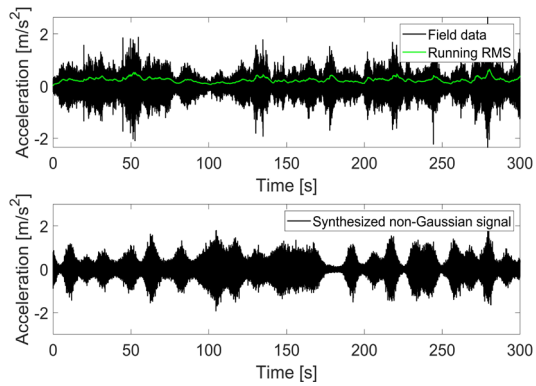


**Fig. 20.** *Field data and synthesized non-Gaussian signal*

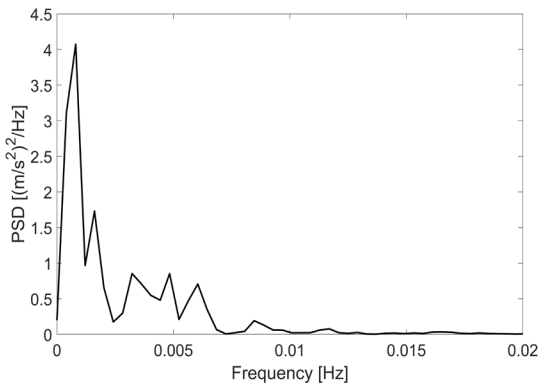


**Fig. 21.** *PSD of running RMS of field data*

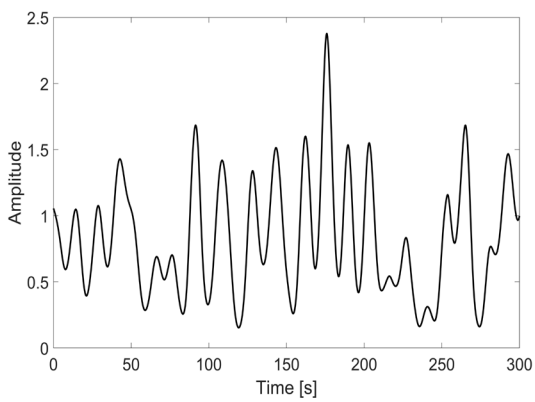


**Fig. 22.** *Simulated AMS with $W_{cut}$ = 0.01*

Fig. 23 shows the PSD of synthesized non-Gaussian signal and field data. Fig. 24 shows the PDF of synthesized non-Gaussian signal and field data in semi-log coordinates. Fig. 25 shows the FDS of synthesized signal and field data ($Q$ = 10 and $b$ = 5). From Figs. 23 to 25, we can observe that a good match is achieved between the PSD, PDF and FDS of synthesized non-Gaussian signal and field data.

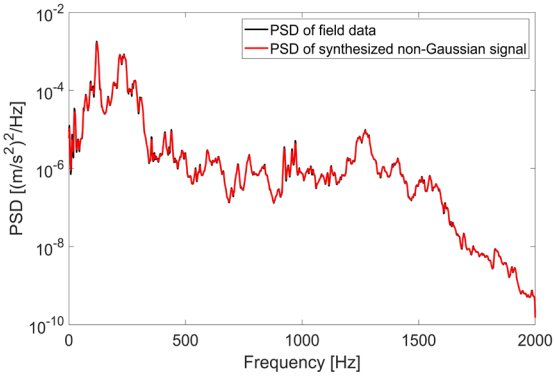


**Fig. 23.** *PSD of field data and synthesized non-Gaussian signals*

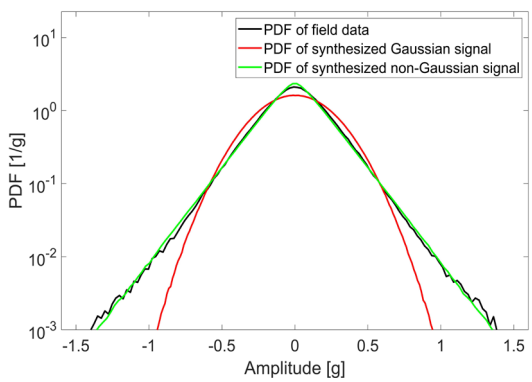


**Fig. 24.** *PDF of field data and synthesized Gaussian and non-Gaussian signals*

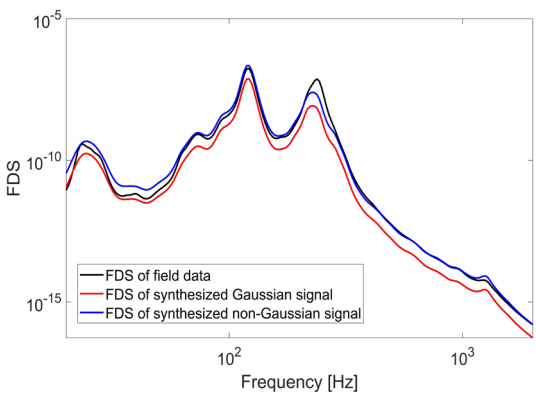


**Fig. 25.** *FDS of field data, synthesized Gaussian and non-Gaussian signals*

## 4 DISCUSSION

The width of the kurtosis range of the amplitude modulation method for non-Gaussian signal generation is enhanced in this study. A linear combination of the AMS modelled by Weibull and Beta distributions is used to address the kurtosis range limitation problem. This study demonstrates that a non-Gaussian signal can be regarded as slowly varying if the running mean value of the AMS during the period of the system impulse response is the same as that of the original AMS. The high kurtosis of the non-Gaussian input signal can be transferred to the linear system response using the proposed AMS control method, in which the spectral content of the AMS is controlled based on the CDF transformation. A higher low-pass cutoff frequency results in a lower kurtosis of the linear response and hence, a lower FDS. Over a practical damping range, it is found that the response of the SDOF system, especially with low natural frequency, to a slowly varying non-Gaussian loading tends to be Gaussian as $Q$ increases. The proposed approach is proven to be effective using simulated and field-measured data.

## 5 ACKNOWLEDGEMENTS

This study was partially supported by The National Natural Science Foundation of China (Grant # 52102443) and the Postgraduate Research & Practice Innovation Program of Yancheng Institute of Technology (Grant # SJCX23_XY050).

## 6 REFERENCES

[1] Bendat, J.S., Piersol, A.G. (2010). *Random Data: Analysis and Measurement Procedures*. John Wiley & Sons, Hoboken, **DOI:10.1002/9781118032428**.

[2] Hui, Y., Li, B., Kawai, H., Yang, Q. (2017). Non-stationary and non-Gaussian characteristics of wind speeds. *Wind and Structures*, vol. 24, no. 1, p. 59-78, **DOI:10.12989/was.2017.24.1.059**.

[3] Steinwolf, A. (2015). Vibration testing of vehicle components by random excitations with increased kurtosis. *International Journal of Vehicle Noise and Vibration*, vol. 11, no. 1, p. 39-66, **DOI:10.1504/IJVNV.2015.067983**.

[4] Han, F., Wang, C., Hu, A. (2017). Numerical investigation of wave-induced vibrations and their effect on the fatigue damage of container ships. *Ocean Engineering*, vol. 142, p. 245-258, **DOI:10.1016/j.oceaneng.2017.06.064**.

[5] STANAG 4370, AECTP-200 (2006). *Mechanical Conditions*. NATO Standardization Agency.

[6] MIL-STD-810H (2019). Department of Defense Test Method Standard: Environmental Engineering Considerations and Laboratory Tests. U.S. Department of Defense, Washington.

[7] DEF STAN 00-35. (2006). *Environmental Handbook for Defence Material: Part 3: Environmental Test Methods*. Ministry of Defence, London.

[8] Steinwolf, A. (2006). Random vibration testing beyond PSD limitations. *Sound and Vibration*, vol. 40, no. 9, p. 12-21.

[9] Steinwolf, A. (2008). Two methods for random shaker testing with low kurtosis. *Sound and Vibration*, vol. 42, no. 10, p. 18-22.

[10] Smallwood, D. (2005). Generating non-Gaussian vibration for testing purposes. *Sound and Vibration*, vol. 39, no. 10, p. 18-23.

[11] Steinwolf, A., Peeters, B., Auweraer, H. (2015). Two methods of generating random excitations with increased kurtosis for in-house testing of vehicle components, *22nd International Congress on Sound and Vibration*.

[12] Steinwolf, A. (2015). Vibration testing of vehicle components by random excitations with increased kurtosis. *International Journal of Vehicle Noise and Vibration*, vol. 11, no. 1, p. 39-66, **DOI:10.1504/IJVNV.2015.067983**.

[13] Yu, Y., Jiang, T. (2007). Generation of non-Gaussian random vibration excitation signal for reliability enhancement test. *Chinese Journal of Aeronautics*, vol. 20, no. 3, p. 236-239, **DOI:10.1016/S1000-9361(07)60038-7**.

[14] Zheng, R., Chen, G.P., Chen, H.H. (2021). Stationary non-Gaussian random vibration control: A review. *Chinese Journal of Aeronautics*, vol. 34, no. 1, p. 350-363, **DOI:10.1016/j.cja.2020.10.005**.

[15] Troncossi, M., Rivola, A. (2014). Response analysis of specimens excited with non-Gaussian acceleration profiles. *Proceedings of ISMA2014*, p. 799-808.

[16] Rizzi, S.A., Przekop, A., Turner, T.L. (2011). On the response of a nonlinear structure to high kurtosis non-Gaussian random loadings. Proceedings of the 8th International Conference on Structural Dynamics, p. 1-8.

[17] Kihm, F., Rizzi, S.A., Ferguson, N.S., Halfpenny, A. (2013). Understanding how kurtosis is transferred from input acceleration to stress response and its influence on fatigue life. *11th International Conference on Recent Advances in Structural Dynamics*, p. 1-16.

[18] Kihm, F., Ferguson, N. S., Antoni, J. (2015). Fatigue life from kurtosis controlled excitations. *Procedia Engineering*, vol.133, p. 698-713, **DOI:10.1016/j.proeng.2015.12.652**.

[19] Smallwood, D. (2009). Vibration with non-Gaussian noise. *Journal of the IEST*, vol. 52, no. 2, p. 13-30, **DOI:10.17764/jiet.52.2.gh0444564n8765k1**.

[20] Xu, F., Li, C., Jiang, T., Ahlin, K. (2015). Synthesis of running rms-induced non-Gaussian random vibration based on Weibull distribution. *Vibroengineering Procedia*, vol. 17, no. 7, p. 3662-3674.

[21] Xu, F., Li, C., Jiang, T. (2016). On the shaker simulation of wind-induced non-Gaussian random vibration. *Shock and Vibration*, vol. 2016, no. 1, 5450865, **DOI:10.1155/2016/5450865**.

[22] Xia, J., Yuan, H., Xu, R. (2019). A new simulation method for non-Gaussian random vibration signals. *Journal of Beijing University of Aeronautics and Astronautics*, vol. 2019, p. 366-372, **DOI:10.13700/j.bh.1001-5965.2018.0299**.

[23] Braccesi, C., Cianetti, F., Palmieri, M.G., Zucca, G. (2018). The importance of dynamic behaviour of vibrating systems on the response in case of non-Gaussian random excitations. *Procedia Structural Integrity*, vol. 12, p. 224-238, **DOI:10.1016/j.prostr.2018.11.092**.

[24] Lalanne, C. (2014). *Mechanical Vibration and Shock Analysis, Fatigue Damage*. John Wiley & Sons, New York.

[25] Cornelis, B., Steinwolf, A., Troncossi, M., Rivola, A. (2015). Shaker testing simulation of nonGaussian random excitations with the fatigue damage spectrum as a criterion of mission signal synthesis. *11th International Conference on Engineering Vibrations*, p. 7-10.

[26] Gaberson, H.A. (2012) Shock severity estimation. *Sound & Vibration*, vol. 46, no. 1, p. 12-20, **DOI:10.1108/13552541211250418**.

[27] Ahlin, K. (2006). Comparison of test specifications and measured field data. *Sound and Vibration*, vol. 40, no. 9, p. 22-25.

[28] Henderson, G.R., Piersol, A.G. (1995). Fatigue damage related descriptor for random vibration test environments. *Sound and Vibration*, vol. 29, no. 10, p. 20-25.

[29] Angeli, A., Cornelis, B., Troncossi, M. (2018). Synthesis of Sine-on-Random vibration profiles for accelerated life tests based on fatigue damage spectrum equivalence. *Mechanical Systems and Signal Processing*, vol. 103, p. 340-351, **DOI:10.1016/j.ymssp.2017.10.022**.

[30] ISO 18431-4. (2007). *Mechanical Vibration and Shock - Signal Processing - Part 4: Shock Response Spectrum Analysis*, International Standard Organization, Geneva.

[31] NAVMAT P-9492 (1979). *Navy Manufacturing Screening Program*. U.S. Navy Department, Washington.